Development/Plasticity/Repair

Axon Initial Segments Are Required for Efficient Motor Neuron Axon Regeneration and Functional Recovery of Synapses

Lindsay H. Teliska,[1] Irene Dalla Costa,[2] Ozlem Sert,[1] Jeffery L. Twiss,[2] and Matthew N. Rasband[1]
[1]Department of Neuroscience, Baylor College of Medicine, Houston, Texas 77030 and [2]Department of Biological Sciences, University of South Carolina, Columbia, South Carolina 29208

The axon initial segment (AIS) generates action potentials and maintains neuronal polarity by regulating the differential trafficking and distribution of proteins, transport vesicles, and organelles. Injury and disease can disrupt the AIS, and the subsequent loss of clustered ion channels and polarity mechanisms may alter neuronal excitability and function. However, the impact of AIS disruption on axon regeneration after injury is unknown. We generated male and female mice with AIS-deficient multipolar motor neurons by deleting AnkyrinG, the master scaffolding protein required for AIS assembly and maintenance. We found that after nerve crush, neuromuscular junction reinnervation was significantly delayed in AIS-deficient motor neurons compared with control mice. In contrast, loss of AnkyrinG from pseudo-unipolar sensory neurons did not impair axon regeneration into the intraepidermal nerve fiber layer. Even after AIS-deficient motor neurons reinnervated the neuromuscular junction, they failed to functionally recover because of reduced synaptic vesicle protein 2 at presynaptic terminals. In addition, mRNA trafficking was disrupted in AIS-deficient axons. Our results show that, after nerve injury, an intact AIS is essential for efficient regeneration and functional recovery of axons in multipolar motor neurons. Our results also suggest that loss of polarity in AIS-deficient motor neurons impairs the delivery of axonal proteins, mRNAs, and other cargoes necessary for regeneration. Thus, therapeutic strategies for axon regeneration must consider preservation or reassembly of the AIS.

Key words: **axon initial segment; cytoskeleton; polarity; regeneration**

Significance Statement

Disruption of the axon initial segment is a common event after nervous system injury. For multipolar motor neurons, we show that axon initial segments are essential for axon regeneration and functional recovery after injury. Our results may help explain injuries where axon regeneration fails, and suggest strategies to promote more efficient axon regeneration.

Introduction

Many nervous system injuries and diseases disrupt axon function. Unfortunately, there are currently no pro-regenerative therapies available since the mechanisms controlling axon regeneration and recovery are not completely understood. Axon regeneration requires the activation of regeneration associated genes, and the delivery of new cytoskeletal proteins, mRNAs, cargoes, and organelles to the growing axon. For example, the local translation of mRNA in axons supports regeneration and survival (Smith et al., 2020) while axotomy increases the influx of mitochondria into the axon (Tamada et al., 2021), perhaps as a mechanism to support the energy demands required for regeneration. In addition, axonal entry of integrins has been proposed to promote axon regeneration (Franssen et al., 2015). However, the mechanisms regulating these pro-regenerative pathways remain poorly understood.

The axon initial segment (AIS) is both the anatomic and physiological transition between somatodendritic and axonal domains. It consists of a high density of voltage-gated sodium and potassium channels anchored to the axonal cytoskeleton through the scaffolding protein AnkyrinG (AnkG) (for recent reviews, see Nelson and Jenkins, 2017; Leterrier, 2018). The clustered ion channels integrate synaptic input to initiate action potentials (Kole et al., 2008). In addition, the AIS maintains neuronal polarity by permitting the entry of axonal cargoes, organelles, and proteins, but exclusion and retrieval of somatodendritic cargoes and proteins back to the soma and dendrites (Nirschl et al., 2017). Given its central role in neuronal

Received June 27, 2022; accepted Aug. 2, 2022.

Author contributions: L.H.T., J.L.T., and M.N.R. designed research; L.H.T., I.D.C., and O.S. performed research; L.H.T., I.D.C., O.S., and M.N.R. analyzed data; L.H.T. wrote the first draft of the paper; L.H.T., I.D.C., J.L.T., and M.N.R. edited the paper; M.N.R. wrote the paper.

This work was supported by National institutes of Health Grant R35 NS122073 to M.N.R.; and the Dr. Miriam and Sheldon G. Adelson Medical Research Foundation to M.N.R. and J.L.T.

The authors declare no competing financial interests.

Correspondence should be addressed to Matthew N. Rasband at rasband@bcm.edu.

https://doi.org/10.1523/JNEUROSCI.1261-22.2022

function, it is not surprising that disease and injury can affect AIS structure and function. For example, mutations in AnkG cause autism and severe intellectual disability (for a recent review, see Stevens and Rasband, 2021), while mutations in AIS ion channels can cause epilepsy (Cooper and Jan, 1999). AISs are disrupted after stroke (Schafer et al., 2009; Hinman et al., 2013), in humans and in mouse models of Alzheimer's disease (Marin et al., 2016; Sohn et al., 2019), after inflammation (Clark et al., 2016), and following axotomy (Tamada et al., 2021). Disruption of the AIS occurs through proteolysis of AnkG and the spectrin cytoskeleton, causing dispersal of AIS membrane proteins (Schafer et al., 2009); loss of clustered ion channels after AIS disruption impairs the ability of neurons to integrate and propagate high-frequency synaptic inputs (Revah et al., 2019). *In vitro* experiments showed that axotomy of hippocampal neurons at or near the AIS can transform a former dendrite into an axon (Gomis-Ruth et al., 2008), and axotomized motor neurons can regenerate through the formation of supernumerary axons (Havton and Kellerth, 1987). Remarkably, loss of the AIS in mature neurons allows somatodendritic proteins to enter the axon causing axons to acquire the molecular and structural features of dendrites, including spines (Hedstrom et al., 2008). Together, these observations show that disrupting the AIS dramatically impacts neuronal function and polarity.

Given the susceptibility of the AIS to injury, and its central role in regulating neuronal polarity, we sought to determine how AIS disruption might influence axon regeneration. We used a nerve crush model to induce axon injury in AIS-deficient mice. We found that axon regeneration and functional recovery were both dramatically impaired in AIS-deficient multipolar motor neurons, but not pseudo-unipolar sensory neurons. Together, our results show that therapeutic approaches aimed at nervous system repair and regeneration must consider preservation or reassembly of the AIS.

Materials and Methods

Animals. *Ank3*$^{f/f}$ mice were generated as previously described (Ho et al., 2014) (catalog #JAX:029797, RRID:IMSR_JAX:029797). *Sptbn4*$^{f/f}$ mice were generated as previously described (Unudurthi et al., 2018). *ChAT-Cre* and *Advillin-Cre* mice were obtained from The Jackson Laboratory (catalog #JAX:006410, RRID:IMSR_JAX:006410 and catalog #JAX:032536, RRID:IMSR_JAX032536, respectively). Both male and female mice were used. All experiments comply with the National Institutes of Health's *Guide for the Care and Use of Laboratory Animals* and were approved by the Baylor College of Medicine Institutional Animal Care and Use Committee.

Antibodies. The mouse monoclonal primary antibodies used for standard immunofluorescence include antibodies against AnkG (clone N106/36, RRID:AB_2877524), NeuN (clone A60, Millipore Sigma catalog #MAB377), and synaptic vesicle protein 2 (SV2) (DSHB catalog #SV2, RRID:AB_2315387). The rabbit polyclonal primary antibodies used for standard immunofluorescence include antibodies against PGP9.5 (Millipore, catalog #AB1761-I, RRID:AB_2868444), Neurofilament-M (NFM, Millipore, catalog #AB1987, RRID:AB_91201), and β4 spectrin (M.N.R. laboratory, RRID:AB_2315634). A chicken polyclonal primary antibody against Neurofascin (R&D Systems, catalog #AF3235, RRID: AB_10890736). α-Bungarotoxin (α-BTX, Thermo Fisher Scientific, catalog #B13422) and Hoechst stain (Thermo Fisher Scientific, catalog #H3569, RRID:AB_2651133) were purchased from Thermo Fisher Scientific. Primary antibodies used in FISH experiments consisted of the following: RT97 mouse anti-neurofilament (NF) (Developmental Studies Hybridoma Bank, RRID AB_528399; 1:200), SMI312 anti-phospho-NF (Biolegend, SMI312, RRID AB_837904; 1:200), and anti-Tubulin β3 (TUJ1; Biolegend, RRID AB_801213; 1:200). Secondary antibodies were purchased from Thermo Fisher Scientific and Jackson ImmunoResearch Laboratories.

Immunofluorescence labeling. Lumbrical muscles were dissected as described previously (Sleigh et al., 2014) and fixed in 4% PFA on ice for 15 min. Muscles were washed in PBS for 5 min, detergent washed in 2% Triton X-100 in PBS for 30 min at room temperature, and finally blocked with 10% normal goat serum in 0.1 M PB with 0.3% Triton X-100 (PBTGS) for 30 min at room temperature. Tissues were incubated in primary antibody solutions diluted in PBTGS overnight at 4°C. The tissues were then washed 3 times in PBTGS, followed by 3 washes in PBS, before incubating in the secondary antibody solution diluted in PBTGS. This was done at room temperature for 2 h. Washes were then repeated as before, and tissues were mounted onto slides and imaged. Spinal cord with dorsal and ventral roots attached were dissected and fixed in 4% PFA on ice for 35 min. Tissues were then moved to 30% sucrose solution in 0.1 M PB at 4°C overnight before sectioning. Glabrous hindpaw skin was dissected and fixed in 4% PFA on ice for 1 h. Tissues were then moved to 30% sucrose solution in 0.1 M PB at 4°C overnight before sectioning. For cryosectioning, tissues were embedded in Tissue-Tek OCT (Sakura Finetek 4583) mounting medium and frozen on dry ice. All tissues were sectioned onto 1% bovine gelatin-precoated coverslips. Spinal cords were sectioned at 25 µm, dorsal and ventral roots at 14 µm, and hindpaw skin at 30 µm. Coverslips were washed with PBS before blocking in PBTGS for 30 min at room temperature. Primary antibody solutions were diluted in PBTGS and incubated overnight at 4°C. The coverslips were then washed 3 times with PBTGS before incubating with the secondary solution (diluted in PBTGS) for 1 h at room temperature. Coverslips were then washed again with PBS and mounted and imaged.

Peripheral nerve injury. A sciatic nerve crush was used to induce peripheral nervous system injury in mice. The left sciatic nerve was crushed at postnatal day 21, and tissue was collected and analyzed at varying time points after crush. The right sciatic nerve served as an internal uninjured control. Animals were administered 1 mg/kg buprenorphine sustained release and meloxicam at a dose of 5 mg/kg and then anesthetized with isoflurane. Hair removal cream (Nair) was applied to the thigh area above the left sciatic nerve for hair removal. The area was then wiped with a 70% ethanol pad and cleaned with betadine scrub. This was repeated 3 times. After ensuring the mouse was anesthetized in the nose cone, a small incision was made above the left sciatic nerve. Once exposed, Dumont No. 3 forceps were used to crush the nerve, proximal to the spinal cord for 10 s. Once injury was complete, the wound was closed with 9 mm wound clips and an antibacterial ointment was applied on the wound to prevent infection.

Compound muscle action potential (CMAP) recording. CMAPs were recorded using a PowerLab signal acquisition system (AD Instruments) as described previously (Zhang et al., 2021). Briefly, mice were anesthetized with isoflurane and placed in a prone position. The anode electrode was subcutaneously placed at the thoracic spinal cord, and the cathode subcutaneously at the lumbar region, near the terminal end of the spinal cord. With the paw pad oriented up, the recording electrode was subcutaneously placed along the plantar skin of the foot and the reference electrode subcutaneously placed in the footpad. Last, the ground electrode was placed subcutaneously at the neck. The sciatic nerve was stimulated with a single pulse of 0.3 ms duration, with supramaximal current ranging up to 10 mA at 1 Hz. Signals were recorded at 40 kHz. LabChart version 8 software was used to analyze CMAP traces. The maximum-minimum values from 10 repeated measurements were averaged to determine the total action potential.

Rotarod. Adult mice were first conditioned on the rotarod (Ugo Basile) at 4 rpm for 5 min. After a 1 h rest, mice were conditioned to an acceleration trial from 4 to 40 rpm over a 5 min period. After a 30 min rest, testing began. Mice were tested for latency to fall in three trials, each separated by a 30 min rest period. The trial consisted of an acceleration period of 4 rpm to 40 rpm over 5 min. Latencies to fall were averaged across the three trials.

FISH. Single-molecule FISH (smFISH) plus immunofluorescence (IF) was used to detect axonal mRNAs in the sciatic nerve. We used custom-designed Cy5-labeled Stellaris probes (LGC Biosearch Tech) for mouse *Nrn1*, *Arc*, and *Gap43* mRNAs (GenBank accession NM_001374754.1, AF162777.1, and NM_008083.2, respectively). A

Cy5-labeled probe targeting *Bacillus subtilis* dihydrodipicolinate reductase (dapB) gene was used as a nonspecific control for the mouse nerve smFISH.

Detection of mRNA in tissues was performed as previously described (Kalinski et al., 2015). Briefly, sciatic nerve segments were fixed for 4 h in 2% buffered PFA at room temperature, cryoprotected overnight in 30% buffered sucrose at 4°C, and then cryosectioned at 12 µm thickness (sections were stored at −20°C until used). All subsequent steps were conducted at room temperature unless specified otherwise. Sections were brought to room temperature, and then treated with 20 mM glycine in PBS 3 times for 10 min each followed by fresh 0.25 M $NaBH_4$ in PBS for 3 times at 5 min each to quench autofluorescence. Sections were quickly rinsed in 0.1 M triethylamine and then incubated in 0.1 M triethylamine + 0.25% acetic anhydride for 10 min. Sections were dehydrated in 70%, 95%, and 100% ethanol (3 min each) and then delipidated in chloroform for 5 min followed by 100% and 95% ethanol (3 min each). After washing in 2× saline-sodium citrate (SSC) buffer, sections were incubated overnight at 37°C in a humidified chamber with 12.5 µM each for test and control RNA probes plus 1:200 each of RT97, TUJ1, and SMI312 in hybridization buffer: 10% dextran sulfate, 1 mg/ml *Escherichia coli* tRNA (Roche), 2 mM vanadyl ribonucleosides (New England Biolabs), 2× SSC, 10% formamide, 1× blocking buffer (Roche). The following day, sections were washed in 2× SSC + 10% formamide at 37°C for 1 h, followed by two incubations in 2× SSC for 5 min each. Sections were briefly rinsed in PBS + 0.3% Triton X-100, and then incubated with secondary antibodies diluted in 1× blocking buffer (Roche) + 0.1% Triton X-100 for 1 h. Sections were finally washed in PBS for 5 min, postfixed in 2% PFA for 15 min, washed 3 times in PBS (5 min each), rinsed in DEPC-treated water, and mounted under glass coverslips using Prolong Gold Anti-fade with DAPI (Thermo Fisher Scientific).

Microscopy. Images for standard immunofluorescence were collected on a Nikon Eclipse Ni-E microscope. In some instances, *Z*-stack images were taken and displayed as maximum intensity projections. Linear contrast and brightness adjustments were performed using Adobe Photoshop. Images were analyzed using Fiji (Schindelin et al., 2012). No other processing of images was performed. smFISH/IF signals were imaged using Leica SP8X confocal microscope with 63×/NA 1.4 oil-immersion objective and pulsed white light laser. Imaging acquisition parameters were determined by settings that gave minimal signals for the nontargeting probe against dapB probe. XYZ image stacks were acquired across at least three separate locations in each section and averaged. Intra-axonal signals were extracted using the Fiji Coloc plugin based on overlap with RT97 + SMI312 + Tuj1 signals across individual *Z* planes. Signals were quantified from larger-diameter axons as visualized from 3D projections using Fiji (National Institutes of Health) as described previously (Kalinski et al., 2015).

Image analyses. To quantify SV2 coverage at the endplate, serial *Z* stacks were taken at 60×. Using Fiji, the average intensity projection was applied to the stack of images. A rectangular ROI was drawn around each neuromuscular junction (NMJ), and the mean background intensity was subtracted for each NMJ ROI. After manually tracing the NMJ, mean fluorescence was measured for SV2 and α-BTX intensities. SV2 intensity was normalized to α-BTX intensity. The postsynaptic morphology of control and conditional KO NMJs was analyzed using an NMJ Morph protocol as described by Zhang et al. (2021). Twelve to 15 NMJs per animal were measured, with 3 animals per condition and genotype. For every animal analyzed, the percentage of NMJ reinnervation after injury was determined by manually counting ~100 NMJs in each lumbrical muscle on the crushed side and uninjured side. The number of nerve endings in the intraepidermal nerve fiber layer was counted manually using Fiji. Branches from one nerve ending were only counted as one nerve ending.

Statistical analyses. Unless otherwise stated, unpaired, two-tailed Student's *t* test was performed for statistical analysis. Data were collected and analyzed using GraphPad Prism and Microsoft Excel. No statistical methods or power analysis was used to predetermine sample sizes, but our sample sizes are similar to those reported previously (Zhang et al., 2021). Data distribution was assumed to be normal.

Results

AnkG conditional KO mice have normal innervation of the NMJ

To determine whether AIS structure and function influence axon regeneration, we generated AIS-deficient spinal motor neurons by crossing *ChAT-Cre* mice with *Ank3*$^{f/f}$ mice; AnkG is the gene product for *Ank3* and is required for the assembly of AIS (Zhou et al., 1998; Hedstrom et al., 2007). We confirmed that *ChAT-Cre;Ank3*$^{f/f}$ spinal motor neurons lack AnkG-labeled AIS (Fig. 1*A*). AnkG was also lost from nodes of Ranvier in ventral motor roots (Fig. 1*B*), but nodes assemble normally because of compensation by AnkR (Ho et al., 2014). However, AnkR cannot compensate for loss of AnkG at AIS (Liu et al., 2020). To determine whether loss of the AIS resulted in motor deficits, we tested motor function using the accelerating rotarod. Surprisingly, we observed no difference between control and *ChAT-Cre;Ank3*$^{f/f}$ mice (Fig. 1*C*), suggesting that AISs are not required for action potential initiation and function in motor neurons. To determine whether motor axon innervation of the NMJ is disrupted in AIS-deficient mice, we immunostained the lumbrical muscles of the foot with the NMJ marker α-BTX and axon marker NFM. We found that NMJs are efficiently innervated in both control and *ChAT-Cre;Ank3*$^{f/f}$ mice (Fig. 1*D*). Nevertheless, morphometric analysis of NMJs showed significant differences in endplate area, compactness, and fragmentation between control and *ChAT-Cre;Ank3*$^{f/f}$ mice (Fig. 1*E–H*), suggesting that loss of neuronal AnkG impacts the differentiation or stabilization of the NMJ. Although mice were grossly normal, we found that many mice spontaneously died at ~4 months of age, likely because of loss of AIS in other CNS cholinergic neurons; thus, we restricted our remaining experiments to mice younger than 4 months. Together, these results show that, although motor neurons in *ChAT-Cre;Ank3*$^{f/f}$ mice lack an AIS, axons still faithfully innervate the NMJ. Furthermore, motor function remains intact despite a perturbed NMJ structure and no AIS.

AIS-deficient axons have impaired regeneration

Since AISs are not required for action potential initiation in spinal motor neurons, we considered whether the motor neuron AIS may instead play a larger role in regulating neuronal polarity (Hedstrom et al., 2008; Sobotzik et al., 2009). We reasoned that disrupted axo-dendritic polarity may have disproportionate effects on regeneration of very long motor axons. To determine how AIS loss affects axon regeneration, we performed sciatic nerve crush to induce axon injury (Fig. 2*A*). We evaluated regeneration by measuring reinnervation of the NMJ and recovery of the CMAP in lumbrical muscles; we used lumbrical muscles since they are the muscles farthest from the site of injury and presumably most difficult to reinnervate. Thus, we evaluated both morphologic and functional recovery. In contrast to some other models of nerve and CNS injury where AISs are lost (Schafer et al., 2009; Tamada et al., 2021), in control mice motor neuron AISs remain intact after sciatic nerve crush (Fig. 2*B*, arrowheads); thus, our strategy of removing AnkG from motor neurons allowed us to test the role of the AIS as a variable independent from the injury itself. Labeling lumbrical muscle NMJs using antibodies against NFM and α-BTX in control mice at 6 and 10 d post crush (DPC) showed no reinnervation in control or *ChAT-Cre;Ank3*$^{f/f}$ mice (data not shown). However, NFM-labeled axons were detected at 66% and 92% of control NMJs, at 14 and 21 DPC, respectively (Fig. 2*C*,*E*). In contrast, we found that *ChAT-Cre;Ank3*$^{f/f}$ mice had significantly impaired regeneration: only 2.8% and 54% of lumbrical muscles were

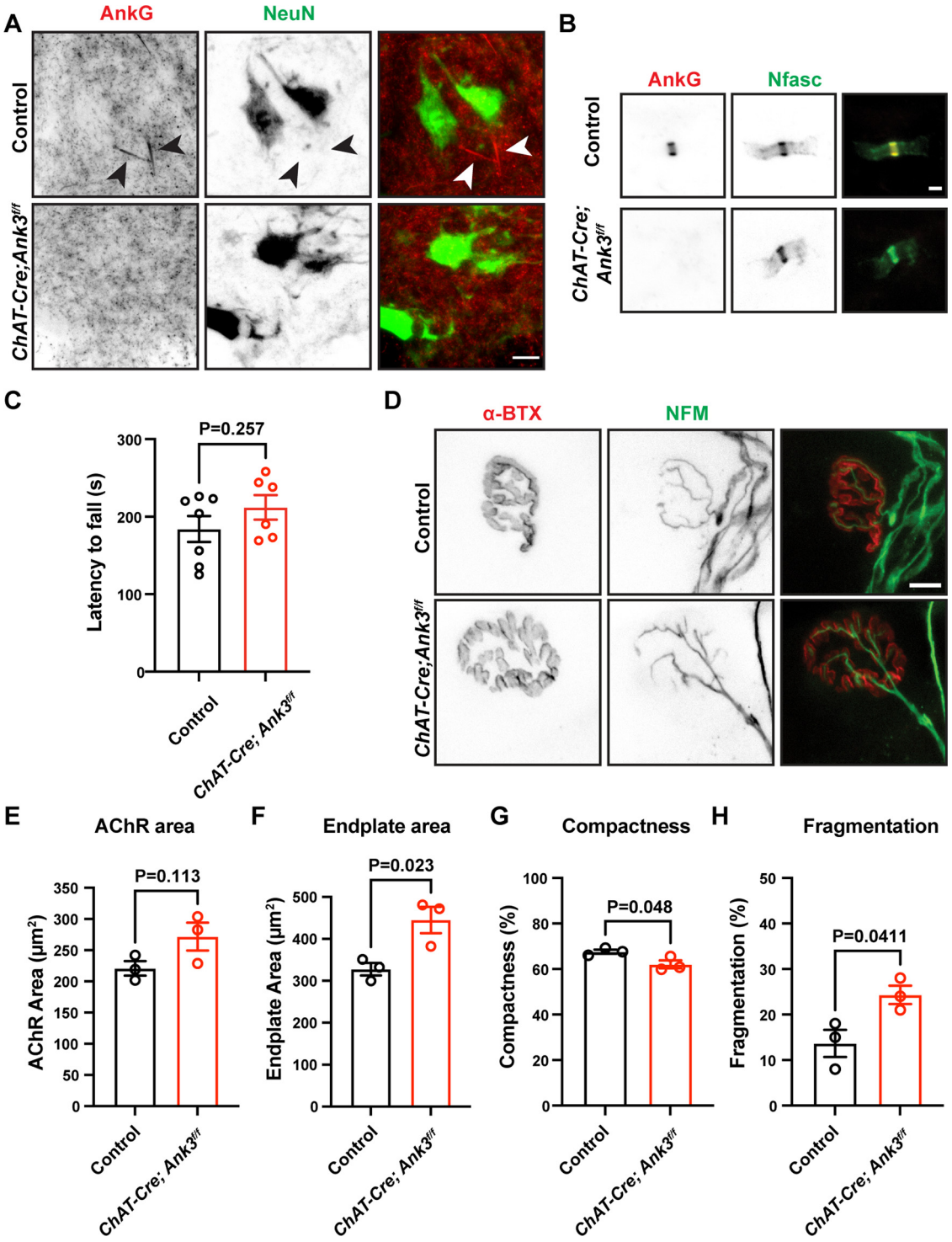

Figure 1. AnkG-deficient motor neurons innervate the NMJ. ***A***, Immunostaining of ventral spinal motor neurons for AnkG (red) and NeuN (green) in control and *ChAT-Cre;Ank3*$^{f/f}$ mice. Arrowheads indicate AnkG-labeled AISs. Scale bar, 20 μm. ***B***, Immunostaining of ventral root nodes of Ranvier for AnkG (red) and Nfasc (green) in control and *ChAT-Cre;Ank3*$^{f/f}$ mice. Scale bar, 2 μm. ***C***, Latency to fall from the rotarod for 2-month-old mice of the indicated genotypes. $N = 6$ or 7 mice. Error bars indicate ±SEM. ***D***, NMJs (labeled by α-BTX in red) are normally innervated in *ChAT-Cre;Ank3*$^{f/f}$ mice. Axons are labeled by NFM (green). Scale bar, 10 μm. ***E–H***, Morphometric analysis of control and *ChAT-Cre;Ank3*$^{f/f}$ NMJs. $N = 3$ mice for both genotypes and all analyses performed, with 12–15 NMJs measured for each animal. Error bars indicate ±SEM.

reinnervated at 14 and 21 DPC, respectively (Fig. 2*D*,*E*). In control mice, NMJ reinnervation recovered completely by 21 DPC, but full NMJ reinnervation in *ChAT-Cre;Ank3*$^{f/f}$ mice did not occur until 35 DPC (Fig. 2*E*). Together, these results show that NMJ reinnervation after injury is significantly delayed in AIS-deficient motor neurons.

AIS-deficient axons have impaired functional recovery

To further investigate whether an intact AIS is important for functional recovery of regenerating axons, we measured CMAPs in control and *ChAT-Cre;Ank3*$^{f/f}$ mice (Fig. 3*A*). Despite normal function on the rotarod (Fig. 1*C*), compared with control mice, we found a consistent reduction in CMAP amplitude in

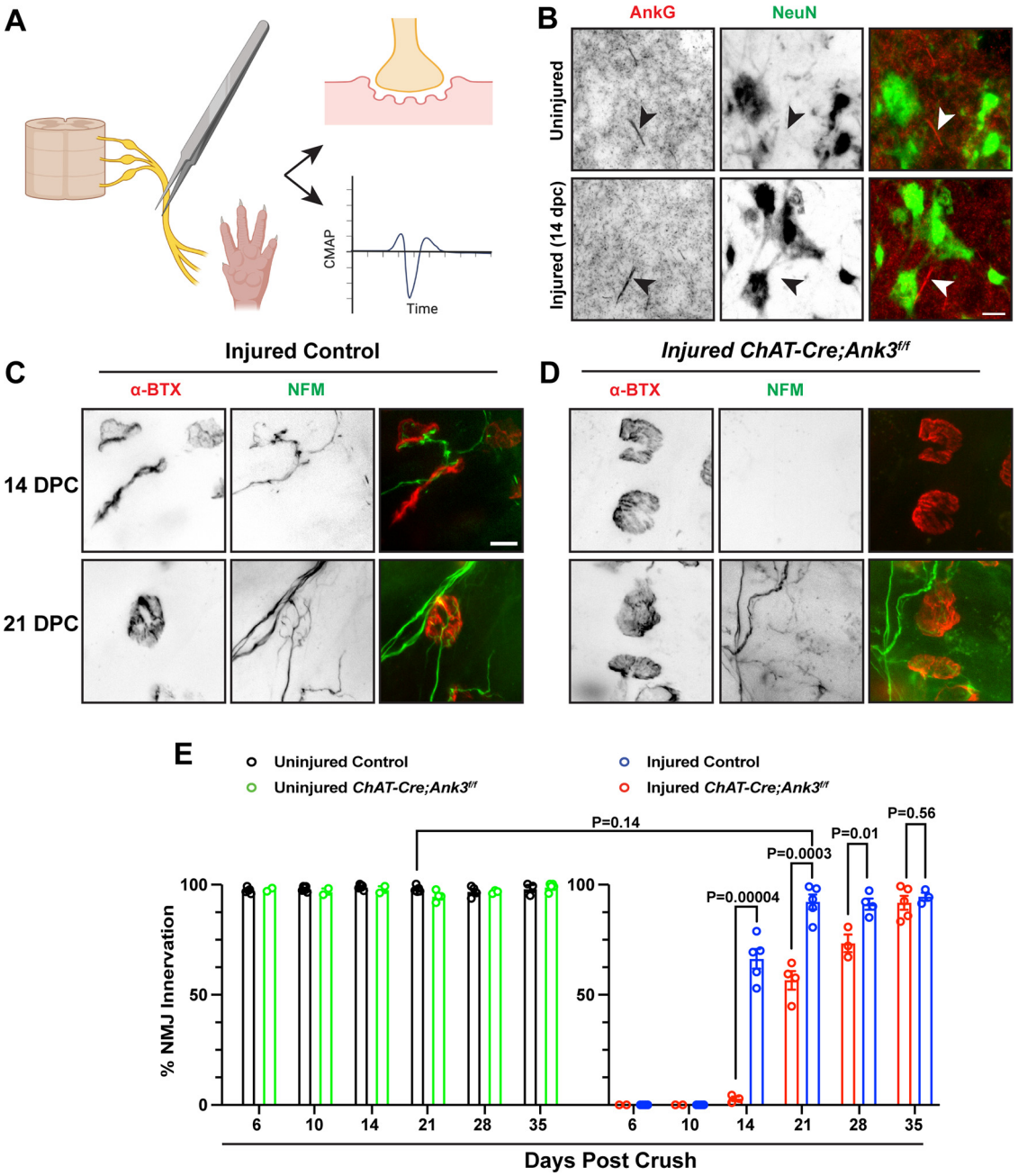

Figure 2. Axon regeneration is delayed in AIS-deficient neurons. ***A***, Schematic represents sciatic nerve crush as a model for axon injury. Motor axon regeneration was evaluated in the lumbrical muscles of the foot at the NMJ. Axon reinnervation of the NMJ was analyzed through immunostaining, while functional recovery of the synapse was analyzed through measuring the CMAP. Created with www.BioRender.com. ***B***, Motor neuron AISs (AnkG, red) are present 14 d after sciatic nerve crush in control mice. NeuN (green) labels neurons. Scale bar, 20 μm. ***C***, Axon reinnervation (NFM, green) of the NMJ (α-BTX, red) in control mice 14 and 21 DPC. Scale bar, 10 μm. ***D***, Axon reinnervation (NFM, green) of the NMJ (α-BTX, red) in *ChAT-Cre;Ank3*$^{f/f}$ mice 14 and 21 DPC. Scale bar, 10 μm. ***E***, Quantification of the percentage of NMJs innervated after injury for the indicated genotypes. $N = 2–5$ mice per time point, with 85-135 NMJs counted per mouse. Error bars indicate ±SEM.

ChAT-Cre;Ank3$^{f/f}$ mice (Fig. 3*B*). This may reflect alterations in NMJ morphology or some other defect in synapse function not detected by measuring performance on the rotarod. After nerve injury and at 14 DPC in both control and *ChAT-Cre;Ank3*$^{F/F}$ mice, CMAPs were completely abolished (Fig. 3*A*,*C*). Since most NMJs in control mice were reinnervated, and postsynaptic acetylcholine receptors are very stable at the motor endplate, this observation suggests that functional recovery of the NMJ requires additional time for maturation of the presynaptic terminal. In control mice, CMAPs returned to normal function by 21 DPC (Fig. 3*A*,*C*). In contrast, CMAPs in *ChAT-Cre;Ank3*$^{f/f}$ mice did not return to pre-injury or control levels even at 35 DPC. Together, these results show that AISs are essential for the functional recovery of regenerating axons.

Destabilizing the AIS delays axon regeneration and recovery

Previous studies showed that AnkG is required for AIS assembly and maintenance (Jenkins and Bennett, 2001; Hedstrom et al., 2008). Our results show that AnkG is also required for efficient axon regeneration and functional recovery. However, not all injuries cause complete loss of AIS proteins. To determine whether a partial disruption of the AIS also affects axon

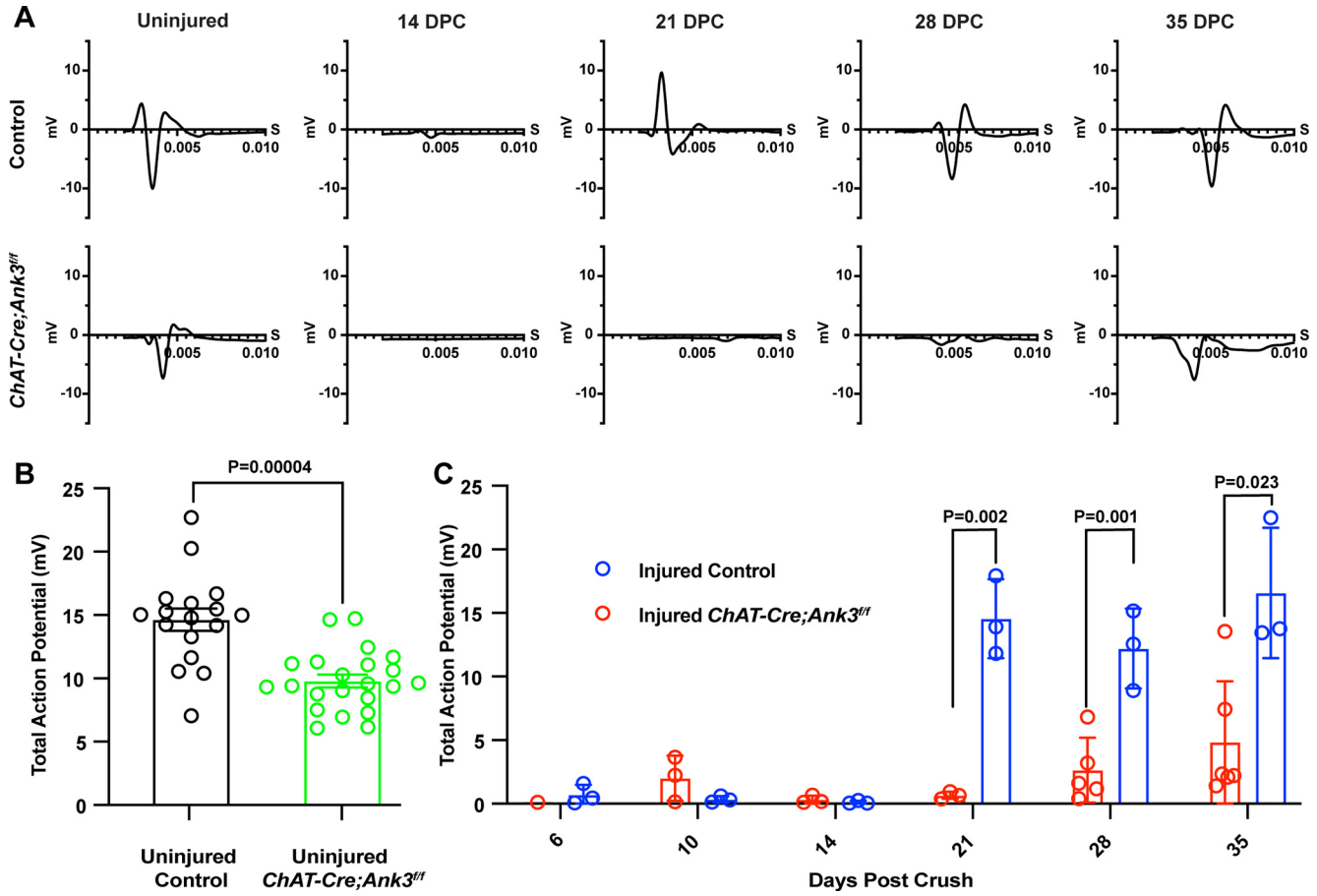

Figure 3. Functional recovery of the NMJ after injury is delayed in AIS-deficient neurons. ***A***, Representative CMAPs from control and *ChAT-Cre;Ank3*$^{f/f}$ mice before and after nerve crush. ***B***, Quantification of the total action potential (mV) in uninjured control and *ChAT-Cre;Ank3*$^{f/f}$ mice. $N = 17$ control and 22 *ChAT-Cre;Ank3*$^{f/f}$ mice. Error bars indicate ±SEM. ***C***, Quantification of the total action potential (mV) in control and *ChAT-Cre;Ank3*$^{f/f}$ mice after nerve crush. $N = 1$–5 mice per genotype at each time point. Error bars indicate ±SEM.

regeneration, we generated mice lacking motor neuron β4 spectrin (*ChAT-Cre;Sptbn4*$^{f/f}$ mice). β4 spectrin-deficient AISs have about half the normal amount of AnkG and Nav channels (Liu et al., 2020). We confirmed that *ChAT-Cre;Sptbn4*$^{f/f}$ spinal motor neurons lack β4 spectrin-labeled AISs (Fig. 4*A*). β4 spectrin was also lost from nodes of Ranvier in ventral motor roots of *ChAT-Cre;Sptbn4*$^{f/f}$ mice (Fig. 4*B*). After nerve crush, we found that β4 spectrin-deficient axons begin to reinnervate lumbrical muscle NMJs by 14 DPC. At 14 DPC, 37% of NMJs are reinnervated in *ChAT-Cre;Sptbn4*$^{f/f}$ mice, compared with only 2.8% in *ChAT-Cre;Ank3*$^{f/f}$ mice and 66% in control mice (Fig. 2*E*). At 21 DPC, 82.31% of NMJs were reinnervated in *ChAT-Cre;Sptbn4*$^{f/f}$ mice (Fig. 4*C*,*D*) compared with only 54% in *ChAT-Cre;Ank3*$^{f/f}$ mice and 92% in control mice. Together, these results show that even intermediate disruption of the AIS can reduce the efficiency of axon regeneration.

Loss of AnkG does not affect regeneration of sensory DRG axons

The sciatic nerve includes both motor and sensory axons. Motor neurons are multipolar with large dendrites and one long axon. In contrast, sensory axons arise from DRG neurons that are pseudo-unipolar, lack dendrites, and project one central and one peripheral axon. One study suggested that most DRG neurons lack an AIS altogether (Gumy et al., 2017), although a more recent study showed that DRG neurons have a bona fide AIS (Nascimento et al., 2022). Nevertheless, the pseudo-unipolar morphology of sensory neurons compared with the multipolar morphology of motor neurons prompted us to consider whether a DRG neuron that does not need to segregate axonal and dendritic cargoes might have less dependence on an AIS for regeneration. Therefore, we analyzed regeneration of AnkG-deficient DRG neurons using *Avil-Cre;Ank3*$^{f/f}$ mice. *Avil-Cre;Ank3*$^{f/f}$ mice lack AnkG at nodes of Ranvier of myelinated dorsal root sensory neurons (Fig. 5*A*). We found that sensory innervation of the intraepidermal nerve fiber layer of the foot was not different between control and *Avil-Cre;Ank3*$^{f/f}$ mice (Fig. 5*B*, arrowheads, Fig. 5*D*). We also measured the reinnervation of the intraepidermal nerve fiber layer after sciatic nerve crush. We found sparse reinnervation at 14 DPC, but regenerating sensory neurons were detected in the intraepidermal nerve fiber layer at 21 and 28 DPC in both control and *Avil-Cre;Ank3*$^{f/f}$ mice (Fig. 5*C*, arrowheads); we measured no difference in the number of nerve fiber endings between control and *Avil-Cre;Ank3*$^{f/f}$ mice (Fig. 5*E*). Together, these results suggest that multipolar neurons, but not pseudo-unipolar neurons, require AnkG and an intact AIS to properly regulate axonal trafficking for efficient axon regeneration.

AIS-deficient nerves have decreased axonal mRNA levels

Localized translation of mRNA in axons has been shown to support developmental growth, regenerative growth, and survival of the axon (Smith et al., 2020). mRNAs and RNA binding proteins typically assemble into granules that bind directly to motor

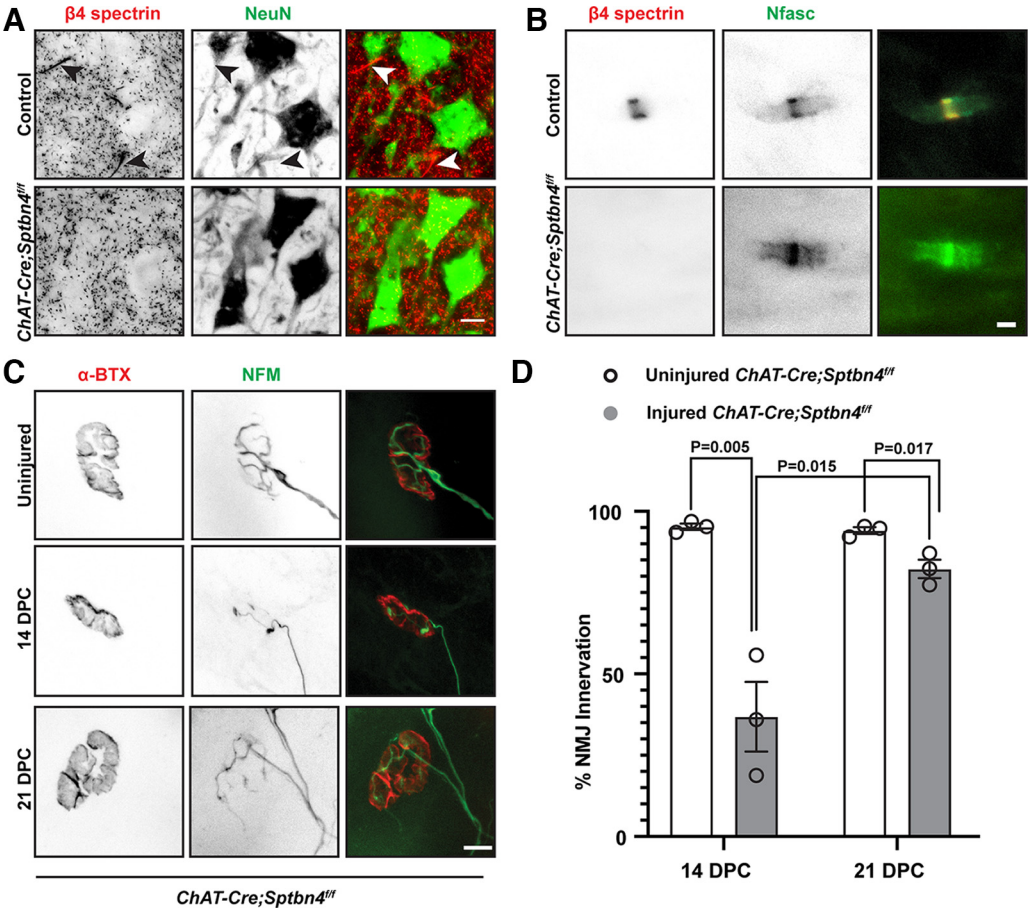

Figure 4. β4 spectrin-deficient neurons have impaired regeneration. ***A***, β4-spectrin (red) is lost from motor neuron AISs in *ChAT-Cre;Sptbn4*$^{f/f}$ mice. NeuN (green) labels neurons. Scale bar, 20 μm. ***B***, *ChAT-Cre;Sptbn4*$^{f/f}$ motor root axons lack nodal β4 spectrin (red). Paranodes and nodes are labeled for neurofascin (green). Scale bar, 2 μm. ***C***, Innervation of NMJs (α-BTX, red) in uninjured and injured *ChAT-Cre;Sptbn4*$^{f/f}$ mice. Axons labeled by NFM (green). Scale bar, 10 μm. ***D***, Quantification of axon innervation in uninjured and injured *ChAT-Cre;Sptbn4*$^{f/f}$ mice at 14 and 21 DPC. $N = 3$ mice per condition and time point, 85–135 NMJs counted per mouse. Error bars indicate ±SEM.

proteins or through adapter proteins or organelles for transport into axons (Dalla Costa et al., 2021). Since the AIS can restrict nonaxonal macromolecules from localization into axons, we tested whether deletion of AnkG might alter mRNA localization. Using smFISH combined with immunofluorescence for neurofilaments and microtubules, we compared the levels of *Nrn1*, *Gap43*, and *Arc* mRNAs that are known to localize into axons, in control and *ChAT-Cre;Ank3*$^{f/f}$ mice at 14 DPC. All three mRNAs showed granular profiles by smFISH that overlapped with neurofilament immunostaining (Fig. 6*A*,*D*,*G*). More diffuse signals were seen outside of the axons, which is likely consistent with the previous reports for Schwann cell expression of *Nrn1* and *Gap43* (Popovic et al., 1996; Min et al., 2012). Extracting the mRNA FISH signals overlapping with neuronal markers across *Z* stacks allowed us to quantify the axonal signals for *Nrn1*, *Gap43*, and *Arc* mRNAs (Kalinski et al., 2015). We focused these analyses on larger-diameter axons as visualized in *Z*-stack projections; comparing the control Cy5-labeled dapB and Cy5-labeled test Stellaris probes allowed us to normalize for nonspecific RNA hybridization signals within each tissue sample. Both in uninjured and crushed nerve samples, the axonal signals for *Nrn1*, *Gap43*, and *Arc* mRNAs were consistently lower in the *ChAT-Cre;Ank3*$^{f/f}$ mice compared with control samples; indeed, *Nrn1* and *Arc* mRNA signals showed very little difference between *ChAT-Cre;Ank3*$^{f/f}$ mice and the dapB probes (Fig. 6*B*,*E*,*H*). Nonetheless, only the *Nrn1* mRNA showed a significant difference, and this was limited to the uninjured nerve samples (Fig. 6*B*,*E*,*H*). However, pooling signals for the uninjured and crushed nerve samples within each genotype showed that the control nerves contained significantly higher axonal signals for *Nrn1*, *Gap43*, and *Arc* mRNAs than nerves from the *ChAT-Cre;Ank3*$^{f/f}$ mice (Fig. 6*C*,*F*,*I*). Together, these data suggest that AIS-deficient motor neurons have reduced axonal transport of *Nrn1*, *Gap43*, and *Arc* mRNAs.

Presynaptic terminals have delayed maturation in regenerating axons of AIS-deficient mice

Despite a delay in reinnervation of the NMJ, the axons of *ChAT-Cre;Ank3*$^{f/f}$ mice eventually reach their targets by 35 DPC (Fig. 2*E*). However, that reinnervation is not accompanied by full functional recovery. Instead, CMAPs remain significantly reduced at 21, 28, and even 35 DPC compared with control mice (Fig. 3*B*). What explains this difference? Since CMAPs depend on successful neuromuscular transmission, and the postsynaptic motor endplate remains intact after injury, we considered whether presynaptic terminals fail to mature in *ChAT-Cre;Ank3*$^{f/f}$ mice. We used immunostaining for SV2 as a surrogate marker for presynaptic differentiation since it is necessary for proper neurotransmission (Ciruelas et al., 2019). Immunostaining of NMJs in uninjured control and uninjured *ChAT-Cre;Ank3*$^{f/f}$ mice showed strong enrichment at the presynaptic terminal (Fig. 7*A*) and no difference in the percentage

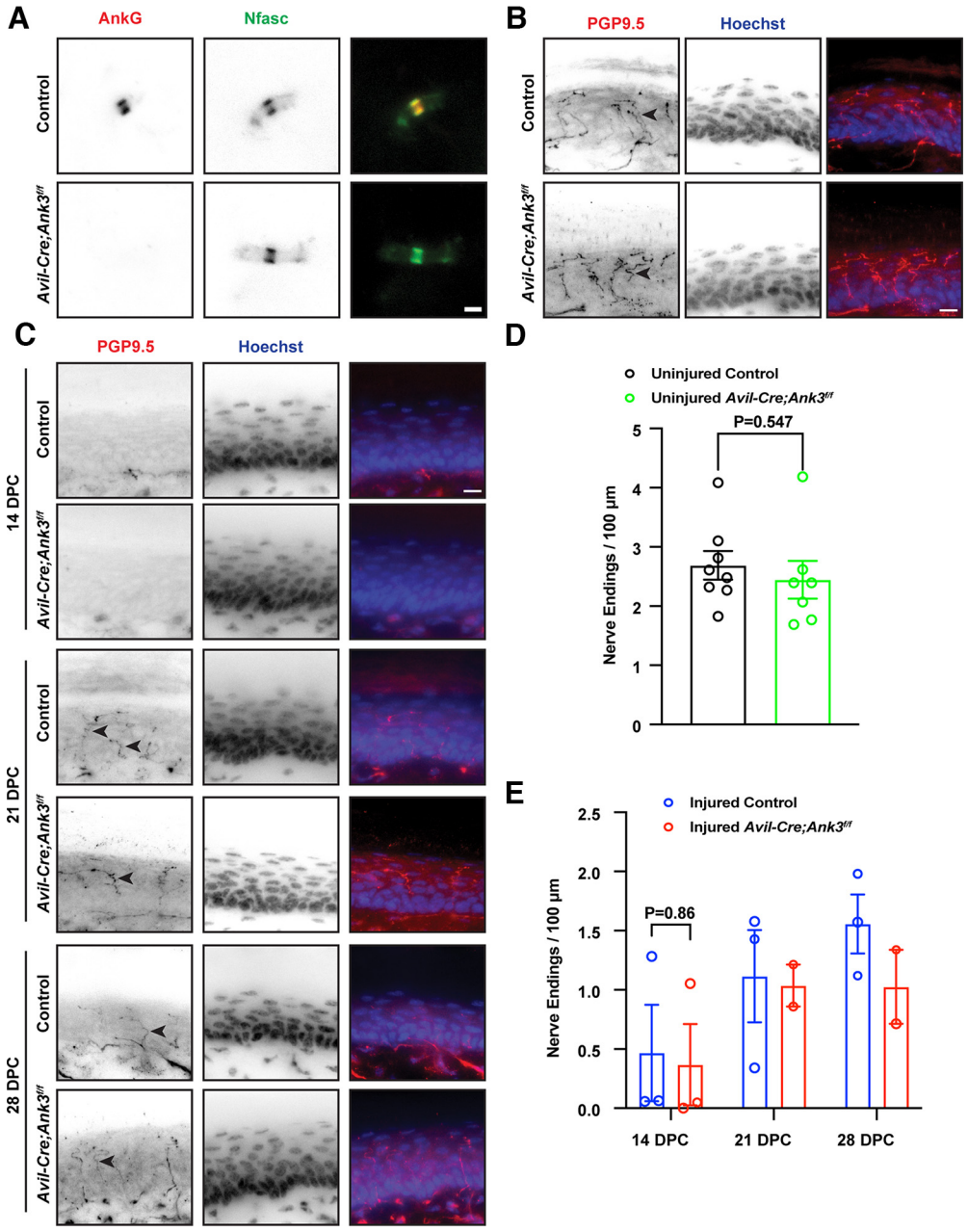

Figure 5. Pseudo-unipolar sensory neurons have normal regeneration. ***A***, *Avil-Cre;Ank3*$^{f/f}$ mice lack AnkG (red) at dorsal root nodes of Ranvier. Paranodes and nodes labeled for neurofascin (green). Scale bar, 2 µm. ***B***, Sensory nerve endings in the intraepidermal nerve fiber layer (labeled by PGP9.5, red, arrowheads) in control and *Avil-Cre;Ank3*$^{f/f}$ mice. Scale bar, 10 µm. ***C***, Regenerating sensory nerve endings in the intraepidermal nerve fiber layer (labeled by PGP9.5, red, arrowheads) in control and *Avil-Cre;Ank3*$^{f/f}$ mice at 14, 21, and 28 DPC. Scale bar, 10 µm. ***D***, Quantification of sensory nerve endings in uninjured control and *Avil-Cre;Ank3*$^{f/f}$ mice in the intraepidermal nerve fiber layer per 100 µm. $N = 7$ or 8 mice per group and condition. Error bars indicate ±SEM. ***E***, Quantification of sensory nerve endings in injured control and *Avil-Cre;Ank3*$^{f/f}$ mice in the intraepidermal nerve fiber layer per 100 µm at 14, 21, and 28 DPC. $N = 2$ or 3 mice per group and condition. Error bars indicate ±SEM or range if $N = 2$.

of SV2 coverage at the motor endplate between control and *ChAT-Cre;Ank3*$^{f/f}$ mice (Fig. 7*C*). To determine whether SV2 is recruited to the NMJ after injury, we immunostained lumbrical muscles from control and *ChAT-Cre;Ank3*$^{f/f}$ mice at 21 DPC (Fig. 7*B*). We found that SV2 immunostaining was significantly reduced at the presynaptic terminals of *ChAT-Cre;Ank3*$^{f/f}$ mice (Fig. 7*D*). The percentage of SV2 coverage at the NMJ was significantly decreased compared with control mice at 21 DPC, a time when injured control mice have normal CMAPs. Nevertheless, we found that SV2 coverage at the nerve terminals recovered to control levels by 35 DPC (Fig. 7*D*) despite impaired functional recovery (Fig. 3*C*). Together, these results show that loss of the AIS delays the molecular maturation of regenerating presynaptic terminals.

Discussion

Diverse nervous system injuries and diseases disrupt the structure and function of the AIS (Huang and Rasband, 2018). Here, we found that AISs are essential for efficient axon regeneration of multipolar motor neurons. AISs are considered mainly as the site where action potentials are generated (Kole et al., 2008), and mice lacking AIS throughout the nervous system die at birth (Ho et al., 2014). Surprisingly, loss of the AIS from motor neurons of

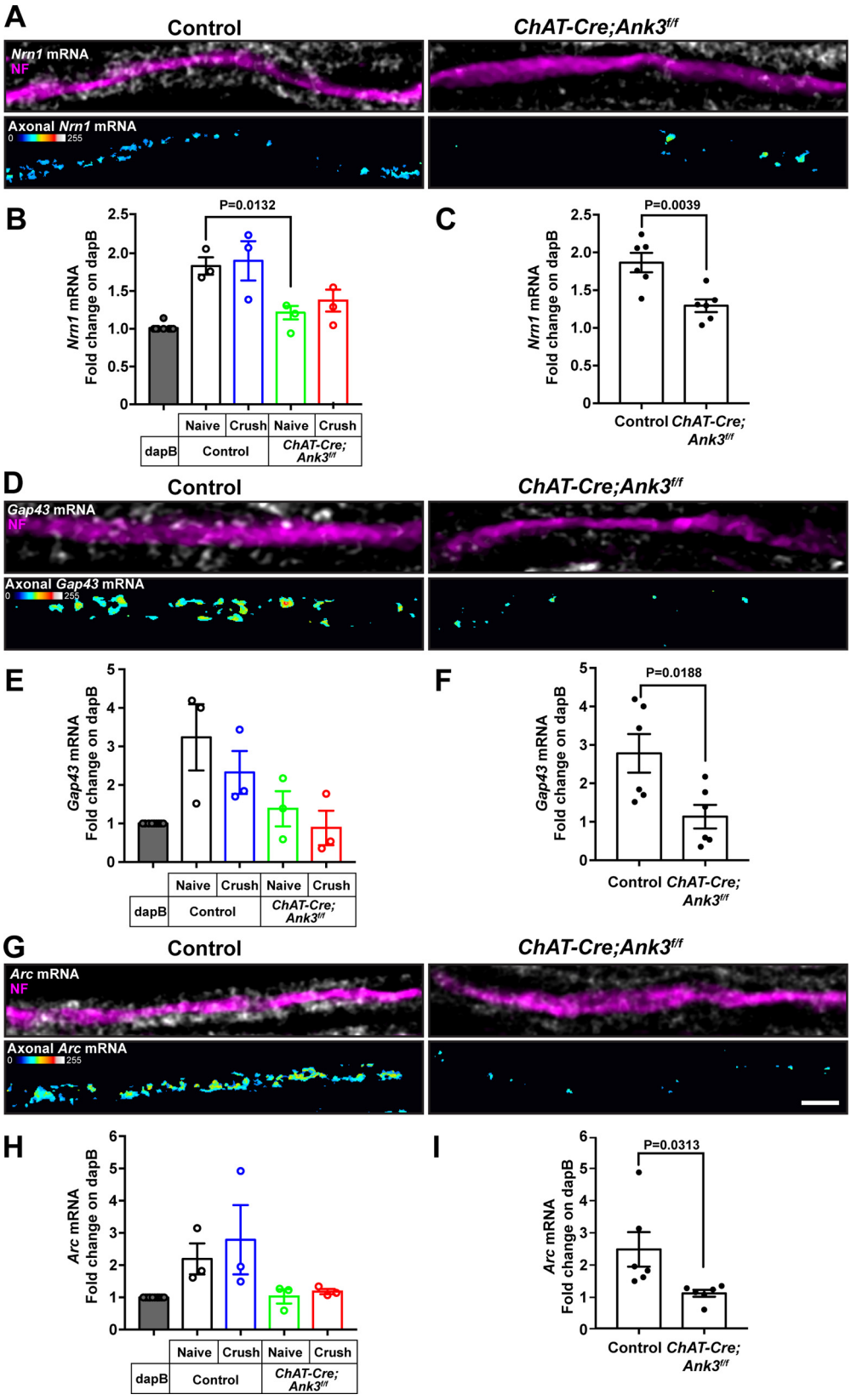

Figure 6. AIS-deficient motor neurons have reduced mRNAs. ***A***, ***D***, ***G***, Representative confocal images for smFISH/IF in uninjured sciatic nerve from control and *ChAT-Cre;Ank3*$^{f/f}$ mice are shown for the indicated mRNAs and RT97 + SMI312 + Tuj1 (collectively referred to as NF). Top panel of each image set represents a single confocal plane of merged signals as indicated. Bottom panel of each image set represents the RNA smFISH signals that overlapped with RT97 + SMI312 + Tuj1 immunofluorescence across individual *Z* planes that are projected as a separate panel and shown as *XYZ* projection (Axonal). Scale bar, 5 μm. ***B***, ***E***, ***H***, Quantification of smFISH signals across multiple mice for uninjured versus 14 DPC sciatic nerve. Samples were normalized for background in each tissue sample by expressing the signals as fold change compared with the nontargeting dapB probe signals. Error bars indicate ±SEM. $N = 3$ nerves per condition. ***C***, ***F***, ***I***, Pooled values are shown for nerves of each genotype as mean ± SEM. $N = 6$ per genotype; data were normally distributed by Shapiro–Wilk test. *p* values were calculated using unpaired Student's *t* test.

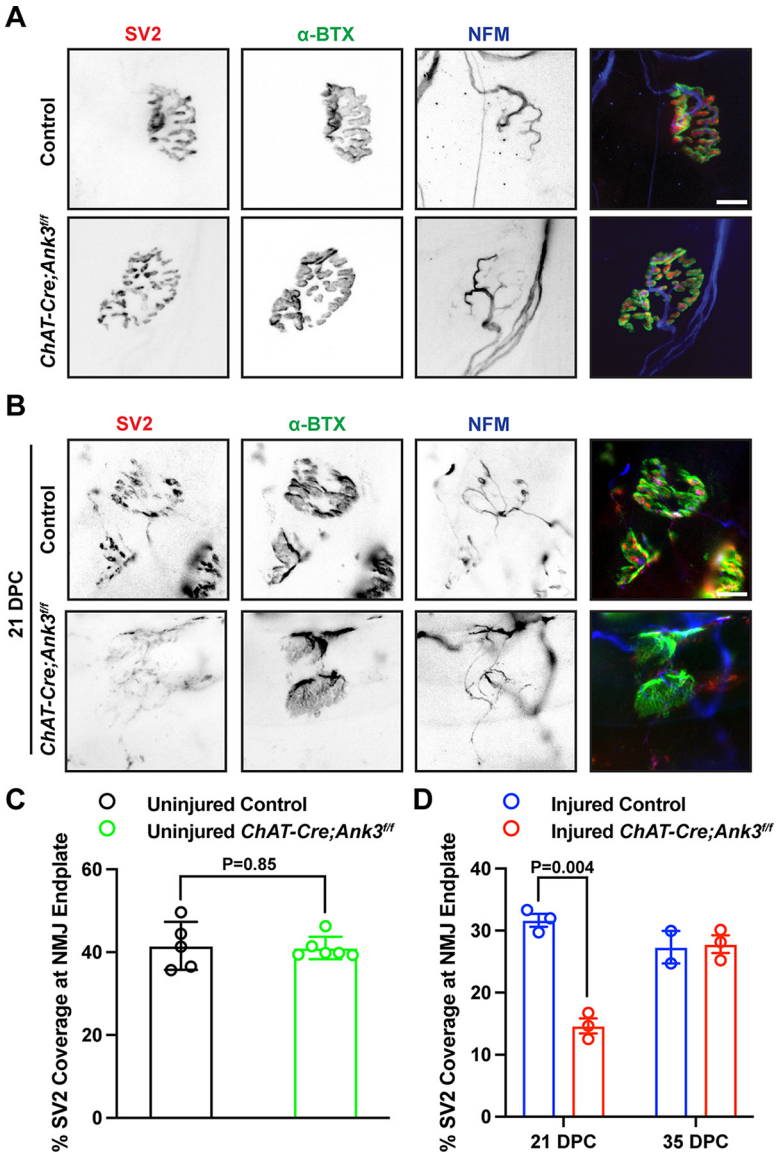

Figure 7. Presynaptic terminal maturation is impaired after injury in AIS-deficient motor neurons. ***A***, Immunostaining of SV2 (red) at the NMJ (α-BTX, green) in control and *ChAT-Cre;Ank3*$^{f/f}$ mice. Axons are labeled for NFM (blue). Scale bar, 10 µm. ***B***, Immunolabeling for SV2 (red) at the NMJ (α-BTX, green) in control and *ChAT-Cre;Ank3*$^{f/f}$ mice at 21 DPC. Scale bar, 10 µm. ***C***, The percentage of SV2 coverage of the NMJ endplate in control and *ChAT-Cre;Ank3*$^{f/f}$ mice at 21 and 35 DPC. $N = 5$ or 6 mice per genotype. Twelve to 15 NMJs were measured per mouse. Error bars indicate ±SEM. ***D***, The percentage of SV2 coverage of the NMJ endplate in control and *ChAT-Cre;Ank3*$^{f/f}$ injured mice at 21 and 35 DPC. $N = 2$ or 3 mice per genotype and condition. Twelve to 15 NMJs were measured per mouse. Error bars indicate ±SEM.

ChAT-Cre;Ank3$^{f/f}$ mice was benign and did not impair motor performance on the rotarod (Fig. 1*C*). Thus, the main function of the AIS in spinal motor neurons is not action potential initiation. We speculate that the resilience of motor neuron action potential initiation may reflect the presence of clustered heminodal Na^+ channels adjacent to the start of the myelin sheath (Duflocq et al., 2011) that can also initiate axonal action potentials. Previous studies showed that the first heminode of layer 5 neocortical neurons facilitates high-frequency firing of action potentials (Kole, 2011). Together, these observations suggest that the failure of AIS-deficient motor neuron axons to efficiently regenerate is unlikely to reflect defects in action potential initiation.

The AIS also functions to maintain neuronal polarity, and the AIS has been described as a barrier or boundary that restricts the entry of proteins, organelles, and cargoes into the axon (Leterrier and Dargent, 2014). Our results are most consistent with the conclusion that loss of the AIS and the subsequent disruption of neuronal polarity is a likely cause of the impaired regeneration in the multipolar motor neuron. This may reflect impaired delivery of proteins and other cargoes to the axon that are important for regeneration, or the aberrant entry of proteins normally restricted to somatodendritic domains. Most prior studies examining how the AIS regulates neuronal polarity investigated the exclusion of somatodendritic proteins and cargoes from the axon. For example, Hedstrom et al. (2008) showed the entry of MAP2 and KCC2 into axons after loss of AnkG. Similarly, other studies showed the exclusion of lipids, and other organelles and vesicles from the axon occurs at the AIS (Winckler et al., 1999; Farias et al., 2015; Balasanyan et al., 2017). However, our experiments suggest that the AIS functions not only as a barrier, but also as a facilitator of axonal trafficking. Specifically, the loss of *Arc*, *Gap43*, and *Nrn1* mRNAs from AIS-deficient motor axons suggests the AIS promotes the entry of specific proteins, mRNAs, and organelles into the axon, many of which are likely important for efficient regeneration. This conclusion is also consistent with our finding that presynaptic maturation is delayed in regenerating axons of *ChAT-Cre;Ank3*$^{f/f}$ mice with reduced levels of presynaptic SV2. The mechanisms that promote axonal targeting of vesicles remain poorly understood but likely depend on the specialized microtubule organization found at the AIS (van Beuningen et al., 2015) and function in coordination with factors that bypass exclusion mechanisms. For example, previous studies suggested that actin patches may function as a barrier mechanism to exclude the trafficking of organelles through the AIS (Watanabe et al., 2012); these patches may be disassembled through actin depolymerization by Mical3. Mical3 is activated by vesicle-bound Rab GTPases, thereby allowing axon-directed cargoes to bypass the AIS (Hamdan et al., 2020). Thus, the failure of axons to efficiently regenerate likely reflects impaired delivery of proteins and cargo because of disrupted neuronal polarity. Future studies should determine the proteins that enter into, or that are excluded from, the regenerating axon. This may provide insights into the mechanisms of axon regeneration, or help determine why axon regeneration is delayed or fails.

Our experiments also showed that impaired regeneration occurred only in motor neurons and loss of AnkG had no effect on regenerating sensory neurons. This observation suggests the larger somatodendritic domain of multipolar motor neurons places greater constraints on the control of trafficking compared with pseudo-unipolar sensory neurons. Nevertheless, other unknown but AnkG-independent mechanisms must also exist to regulate the differential trafficking of proteins and organelles to central and peripheral branches of the pseudo-unipolar sensory neuron. Whereas differential trafficking mechanisms in multipolar neurons are found at the AIS, in pseudo-unipolar sensory neurons, these trafficking decisions must occur at the intersection and branch point connecting the central, peripheral,

and stem branches of the sensory DRG neuron. Intriguingly, this site is also a node of Ranvier and shares many of the same molecular components as the AIS. Additional studies will be needed to better understand the mechanisms controlling polarized trafficking in peripheral sensory neurons.

Why does loss of the AIS alone not affect NMJ innervation in uninjured AIS-deficient motor neurons? One previous study reported axon degeneration after loss of AnkG using *SLICK-H-CreER* mice (Saifetiarova et al., 2017). However, we found no axon degeneration in AnkG-deficient motor or sensory neurons since nodes of Ranvier were normal, and we did not detect any βAPP, caspase-3, or ATF3 immunoreactivity in AIS-deficient neurons (all markers of axon degeneration; data not shown). Although AnkR can compensate for AnkG at nodes of Ranvier, it cannot compensate at AIS (Ho et al., 2014; Liu et al., 2020). Nevertheless, axons innervated NMJs normally (Fig. 1*D*). Although the reasons for the difference between our results and those of Saifetiarova et al. (2017) are unclear, they likely reflect the different *Cre* lines or timing of recombination. Indeed, AISs are not required for the initial specification of the axon (Galiano et al., 2012), and the neuron may become sensitive to loss of the AIS only after distal targets have been reached.

We previously showed that AIS disruption can occur through proteolysis by calpains (Schafer et al., 2009). A primary target of calpain is the spectrin-based cytoskeleton, and β4 spectrin is highly enriched at the AIS. Although some nervous system injuries can completely disrupt the AIS, others may not entirely dismantle the AIS but only reduce its efficiency. We modeled this situation using *ChAT-Cre;Sptbn4*$^{f/f}$ mice and found that, although regeneration was not as impaired as the *ChAT-Cre;Ank3*$^{f/f}$ mice, it was still delayed. This is important since any delay in axon regeneration after injury can have significant consequences for functional recovery when regeneration must occur over long distances. Indeed, one of the major limitations to successful reinnervation and regeneration of peripheral nerves in humans is the rate of axon regeneration. Our results suggest that any injury that even partially disrupts the AIS may have significant consequences for repair.

In conclusion, we describe an important role for the AIS in axon regeneration in multipolar neurons, primarily because of its control over neuronal polarity. We show that the AIS not only functions as a barrier to entry of somatodendritic proteins, but the AIS also facilitates the entry of axonal mRNAs and proteins. Finally, our results suggest that any therapeutic effort aimed at axon regeneration must also consider the preservation or repair of the AIS.

References

Balasanyan V, Watanabe K, Dempsey WP, Lewis TL Jr, Trinh LA, Arnold DB (2017) Structure and function of an actin-based filter in the proximal axon. Cell Rep 21:2696–2705.

Ciruelas K, Marcotulli D, Bajjalieh SM (2019) Synaptic vesicle protein 2: a multi-faceted regulator of secretion. Semin Cell Dev Biol 95:130–141.

Clark KC, Josephson A, Benusa SD, Hartley RK, Baer M, Thummala S, Joslyn M, Sword BA, Elford H, Oh U, Dilsizoglu-Senol A, Lubetzki C, Davenne M, DeVries GH, Dupree JL (2016) Compromised axon initial segment integrity in EAE is preceded by microglial reactivity and contact. Glia 64:1190–1209.

Cooper EC, Jan LY (1999) Ion channel genes and human neurological disease: recent progress, prospects, and challenges. Proc Natl Acad Sci USA 96:4759–4766.

Dalla Costa I, Buchanan CN, Zdradzinski MD, Sahoo PK, Smith TP, Thames E, Kar AN, Twiss JL (2021) The functional organization of axonal mRNA transport and translation. Nat Rev Neurosci 22:77–91.

Duflocq A, Chareyre F, Giovannini M, Couraud F, Davenne M (2011) Characterization of the axon initial segment (AIS) of motor neurons and identification of a para-AIS and a juxtapara-AIS, organized by protein 4.1B. BMC Biol 9:66.

Farias GG, Guardia CM, Britt DJ, Guo X, Bonifacino JS (2015) Sorting of dendritic and axonal vesicles at the pre-axonal exclusion zone. Cell Rep 13:1221–1232.

Franssen EH, Zhao RR, Koseki H, Kanamarlapudi V, Hoogenraad CC, Eva R, Fawcett JW (2015) Exclusion of integrins from CNS axons is regulated by Arf6 activation and the AIS. J Neurosci 35:8359–8375.

Galiano MR, Jha S, Ho TS, Zhang C, Ogawa Y, Chang KJ, Stankewich MC, Mohler PJ, Rasband MN (2012) A distal axonal cytoskeleton forms an intra-axonal boundary that controls axon initial segment assembly. Cell 149:1125–1139.

Gomis-Ruth S, Wierenga CJ, Bradke F (2008) Plasticity of polarization: changing dendrites into axons in neurons integrated in neuronal circuits. Curr Biol 18:992–1000.

Gumy LF, Katrukha EA, Grigoriev I, Jaarsma D, Kapitein LC, Akhmanova A, Hoogenraad CC (2017) MAP2 defines a pre-axonal filtering zone to regulate KIF1- versus KIF5-dependent cargo transport in sensory neurons. Neuron 94:347–362.e7.

Hamdan H, Lim BC, Torii T, Joshi A, Konning M, Smith C, Palmer DJ, Ng P, Leterrier C, Oses-Prieto JA, Burlingame AL, Rasband MN (2020) Mapping axon initial segment structure and function by multiplexed proximity biotinylation. Nat Commun 11:100.

Havton L, Kellerth JO (1987) Regeneration by supernumerary axons with synaptic terminals in spinal motoneurons of cats. Nature 325:711–714.

Hedstrom KL, Xu X, Ogawa Y, Frischknecht R, Seidenbecher CI, Shrager P, Rasband MN (2007) Neurofascin assembles a specialized extracellular matrix at the axon initial segment. J Cell Biol 178:875–886.

Hedstrom KL, Ogawa Y, Rasband MN (2008) AnkyrinG is required for maintenance of the axon initial segment and neuronal polarity. J Cell Biol 183:635–640.

Hinman JD, Rasband MN, Carmichael ST (2013) Remodeling of the axon initial segment after focal cortical and white matter stroke. Stroke 44:182–189.

Ho TS, Zollinger DR, Chang KJ, Xu M, Cooper EC, Stankewich MC, Bennett V, Rasband MN (2014) A hierarchy of ankyrin-spectrin complexes clusters sodium channels at nodes of Ranvier. Nat Neurosci 17:1664–1672.

Huang CY, Rasband MN (2018) Axon initial segments: structure, function, and disease. Ann NY Acad Sci 1420:46–61.

Jenkins SM, Bennett V (2001) Ankyrin-G coordinates assembly of the spectrin-based membrane skeleton, voltage-gated sodium channels, and L1 CAMs at Purkinje neuron initial segments. J Cell Biol 155:739–746.

Kalinski AL, Sachdeva R, Gomes C, Lee SJ, Shah Z, Houle JD, Twiss JL (2015) mRNAs and protein synthetic machinery localize into regenerating spinal cord axons when they are provided a substrate that supports growth. J Neurosci 35:10357–10370.

Kole MH (2011) First node of Ranvier facilitates high-frequency burst encoding. Neuron 71:671–682.

Kole MH, Ilschner SU, Kampa BM, Williams SR, Ruben PC, Stuart GJ (2008) Action potential generation requires a high sodium channel density in the axon initial segment. Nat Neurosci 11:178–186.

Leterrier C (2018) The axon initial segment: an updated viewpoint. J Neurosci 38:2135–2145.

Leterrier C, Dargent B (2014) No Pasaran! Role of the axon initial segment in the regulation of protein transport and the maintenance of axonal identity. Semin Cell Dev Biol 27:44–51.

Liu CH, Seo R, Ho TS, Stankewich M, Mohler PJ, Hund TJ, Noebels JL, Rasband MN (2020) β spectrin-dependent and domain specific mechanisms for Na^+ channel clustering. Elife 9:e56629.

Marin MA, Ziburkus J, Jankowsky J, Rasband MN (2016) Amyloid-beta plaques disrupt axon initial segments. Exp Neurol 281:93–98.

Min S, Jian-bo L, Hong-man Z, Ling-fei Y, Min X, Jia-wei C (2012) Neuritin is expressed in Schwann cells and down-regulated in apoptotic Schwann cells under hyperglycemia. Nutr Neurosci 15:264–270.

Nascimento AI, Da Silva TF, Fernandes EC, Luz LL, Mar FM, Safronov BV, Sousa MM (2022) Sensory neurons have an axon initial segment that initiates spontaneous activity in neuropathic pain. Brain 145:1632–1640.

Nelson AD, Jenkins PM (2017) Axonal membranes and their domains: assembly and function of the axon initial segment and node of Ranvier. Front Cell Neurosci 11:136.

Nirschl JJ, Ghiretti AE, Holzbaur EL (2017) The impact of cytoskeletal organization on the local regulation of neuronal transport. Nat Rev Neurosci 18:585–597.

Popovic M, Sketelj J, Bresjanac M (1996) Changes of Schwann cell antigenic profile after peripheral nerve injury. Pflugers Arch 431:R287–R288.

Revah O, Stoler O, Neef A, Wolf F, Fleidervish IA, Gutnick MJ (2019) Dynamic gain analysis reveals encoding deficiencies in cortical neurons that recover from hypoxia-induced spreading depolarizations. J Neurosci 39:7790–7800.

Saifetiarova J, Taylor AM, Bhat MA (2017) Early and late loss of the cytoskeletal scaffolding protein, ankyrin G reveals its role in maturation and maintenance of nodes of Ranvier in myelinated axons. J Neurosci 37:2524–2538.

Schafer DP, Jha S, Liu F, Akella T, McCullough LD, Rasband MN (2009) Disruption of the axon initial segment cytoskeleton is a new mechanism for neuronal injury. J Neurosci 29:13242–13254.

Schindelin J, Arganda-Carreras I, Frise E, Kaynig V, Longair M, Pietzsch T, Preibisch S, Rueden C, Saalfeld S, Schmid B, Tinevez JY, White DJ, Hartenstein V, Eliceiri K, Tomancak P, Cardona A (2012) Fiji: an open-source platform for biological-image analysis. Nat Methods 9:676–682.

Sleigh JN, Burgess RW, Gillingwater TH, Cader MZ (2014) Morphological analysis of neuromuscular junction development and degeneration in rodent lumbrical muscles. J Neurosci Methods 227:159–165.

Smith TP, Sahoo PK, Kar AN, Twiss JL (2020) Intra-axonal mechanisms driving axon regeneration. Brain Res 1740:146864.

Sobotzik JM, Sie JM, Politi C, Del Turco D, Bennett V, Deller T, Schultz C (2009) AnkyrinG is required to maintain axo-dendritic polarity in vivo. Proc Natl Acad Sci USA 106:17564–17569.

Sohn PD, Huang CT, Yan R, Fan L, Tracy TE, Camargo CM, Montgomery KM, Arhar T, Mok SA, Freilich R, Baik J, He M, Gong S, Roberson ED, Karch CM, Gestwicki JE, Xu K, Kosik KS, Gan L (2019) Pathogenic tau impairs axon initial segment plasticity and excitability homeostasis. Neuron 104:458–470.e5.

Stevens SR, Rasband MN (2021) Ankyrins and neurological disease. Curr Opin Neurobiol 69:51–57.

Tamada H, Kiryu-Seo S, Sawada S, Kiyama H (2021) Axonal injury alters the extracellular glial environment of the axon initial segment and allows substantial mitochondrial influx into axon initial segment. J Comp Neurol 529:3621–3632.

Unudurthi SD, Nassal D, Greer-Short A, Patel N, Howard T, Xu X, Onal B, Satroplus T, Hong D, Lane C, Dalic A, Koenig SN, Lehnig AC, Baer LA, Musa H, Stanford KI, Smith S, Mohler PJ, Hund TJ (2018) βIV-Spectrin regulates STAT3 targeting to tune cardiac response to pressure overload. J Clin Invest 128:5561–5572.

van Beuningen SF, et al. (2015) TRIM46 controls neuronal polarity and axon specification by driving the formation of parallel microtubule arrays. Neuron 88:1208–1226.

Watanabe K, Al-Bassam S, Miyazaki Y, Wandless TJ, Webster P, Arnold DB (2012) Networks of polarized actin filaments in the axon initial segment provide a mechanism for sorting axonal and dendritic proteins. Cell Rep 2:1546–1553.

Winckler B, Forscher P, Mellman I (1999) A diffusion barrier maintains distribution of membrane proteins in polarized neurons. Nature 397:698–701.

Zhang C, Joshi A, Liu Y, Sert O, Haddix SG, Teliska LH, Rasband A, Rodney GG, Rasband MN (2021) Ankyrin-dependent Na(+) channel clustering prevents neuromuscular synapse fatigue. Curr Biol 31:3810–3819.e4.

Zhou D, Lambert S, Malen PL, Carpenter S, Boland LM, Bennett V (1998) AnkyrinG is required for clustering of voltage-gated Na channels at axon initial segments and for normal action potential firing. J Cell Biol 143:1295–1304.